Available online at www.sciencedirect.com
SCIENCE DIRECT®
ELSEVIER
International Journal of Impact Engineering 32 (2005) 575–592
INTERNATIONAL JOURNAL OF IMPACT ENGINEERING
www.elsevier.com/locate/ijimpeng

Dynamic buckling of thin cylindrical shells under axial impact

Z.G. Wei[a,b], J.L. Yu[a,*], R.C. Batra[b]

[a]*CAS Key Laboratory of Mechanical Behavior and Design of Materials, University of Science and Technology of China, Hefei 230027, Anhui, PR China*
[b]*Department of Engineering Science and Mechanics, MC 0219, Virginia Polytechnic Institute and State University, Blacksburg, VA 24061, USA*

Received 16 September 2004; received in revised form 10 June 2005; accepted 21 July 2005

Abstract

The dynamic buckling of thin isotropic thermoviscoplastic cylindrical shells compressed with a uniform axial velocity prescribed at the end faces is investigated analytically and numerically. In the first part of the paper, the stressed/deformed state of a shell is assumed to have buckled if infinitesimal perturbations superimposed upon it grow. Cubic algebraic equations are derived for both the initial growth rate of the perturbation and its wavenumber. The wavenumber corresponding to the maximum initial growth rate of a perturbation introduced at an axial strain of 0.1 is taken to determine the buckling mode. The computed buckling modes are found to match well with those listed in the available experimental data. A thermoviscoplastic constitutive relation is used to delineate the influence of material parameters on the buckling behavior. In the second part of the paper, the finite element method is used to analyze the collapse of an imperfect circular cylindrical tube with axial velocity prescribed at one of its flat end faces with the other end face kept fixed. The influence of initial randomly located imperfections on the buckling behavior is investigated and discussed.
© 2005 Elsevier Ltd. All rights reserved.

Keywords: Instability; Imperfections; Thermoviscoplastic material; Collapse; Perturbation method

*Corresponding author. Tel.: +86 551 360 3793; fax: +86 551 360 6459.
E-mail address: jlyu@ustc.edu.cn (J.L. Yu).

0734-743X/$ - see front matter © 2005 Elsevier Ltd. All rights reserved.
doi:10.1016/j.ijimpeng.2005.07.008

1. Introduction

Thin-walled circular cylindrical shells are used widely as energy absorbing devices since they are inexpensive, efficient and reliable. It is important to examine various features of their response in order to predict the energy-absorbing property and to estimate the associated crushing forces. An understanding of axial crushing of thin-walled shells under quasi-static loading has been well established over the past two decades [1]. Generally, due to very low rate of deformation, the inertia and strain rate effects play a negligible role and the progressive buckling mode is obtained. The progressive buckling under a quasi-static load results in folds that generally occur at one end of the shell, though these folds may appear in different forms, such as axisymmetric, concertina, and mixed mode. When a shell is subjected to a sudden axial load, the response is dynamic plastic buckling, which may be quite different from progressive buckling. Wrinkling will occur along a large portion of the length, and folds may also occur if the load is severe enough. The energy-absorbing characteristics of elastic–plastic shells under impact are often associated with folding mechanism of deformation [1–6]. A comprehensive review of progressive and dynamic buckling is given in [1].

Historically, dynamic plastic buckling is associated with high velocity impact of cylindrical shells made of an aluminum alloy [7,8]. When cylindrical shells are subjected to axial impact at speeds sufficient to cause a moderate amount of plastic deformation axisymmetric buckling occurs. Experiments on 6061-T6 aluminum cylindrical shells showed that the wavelengths of buckled cylinders were uniform along the length and buckled shapes were reproducible. Similar plastic instabilities have been observed in rods and plates subjected to impact or impulsive loads. Abrahamson and Goodier [9] investigated the plastic buckling of rods caused by axial impact. They defined amplification factor as the ratio of the maximum amplitude of the shape imperfection associated with the nth mode to its average value, and postulated that the structure buckled when the amplification factor exceeded a prespecified value, say 10. This method has been successfully used to analyze plastic buckling of rods caused by axial impact [9], plastic buckling of plates due to in-plane forces [10], and plastic buckling of cylindrical shells under axial impact [7]. Wang and Ru [11] used the following energy criterion for analyzing the dynamic buckling of a structure. The structure is unstable if under a kinematically admissible perturbation superimposed on the dominant motion, the work done by internal stresses is less than the work done by external forces. The energy criterion has been applied to study the radial buckling of cylindrical shells by Gu et al. [12]. Batra and Wei [13] have postulated that the buckling mode corresponds to the wavelength of the superimposed perturbation that has the maximum initial growth rate, and have used it to study the buckling of a thin anisotropic thermoviscoplastic plate due to inplane forces.

Dynamic plastic buckling has been associated with high velocity impacts, while progressive buckling has been assumed for low-velocity impacts [1]. However, some experiments on aluminum shells subjected to high-velocity impacts, e.g. see [14], also registered progressive buckling, which means that the dynamic plastic buckling cannot be associated only with the influence of inertia effects. The experimental study in [15] shows that a variety of dynamic buckling response of axially loaded shells is caused by coupling of the inertia effect with the inelastic material properties. Dynamic elastic–plastic buckling is a complex phenomenon which is sensitive to inertia and strain rate effects as shown in [16–18].

Recent developments in axisymmetric buckling of circular cylindrical shells have generated interest in the effects of stress wave propagation [19–22]. It is reported that the inertia characteristics of the shell, together with the material properties, determine particular patterns of the axial stress propagation thus causing either dynamic plastic or dynamic progressive buckling to develop. These simulations did not consider the effect of initial imperfections.

In the first part of the paper we use a perturbation method to analyze the buckling of simply supported thin cylindrical shells under high speed axial impact. The influence of density, specific heat, strain hardening, strain-rate sensitivity, thermal softening of material, the applied strain rate, the shell-wall thickness and the mean radius of the shell on the wavelength of the buckled shape is investigated. Subsequently, the buckling of circular cylindrical aluminum shells under low-speed axial impact is studied using the finite element method and the influence of imperfections is investigated.

2. Dynamic plastic buckling analyzed by the perturbation method

2.1. Formulation of the problem

The dynamic elastic–plastic buckling of structures is a complex phenomenon, due to various factors such as inertia effects, large deformations, and inelastic behavior. It is thus not possible to obtain analytical solutions in general cases, so simplified models are necessary for analysis. Following [1,7,8], it is assumed that during deformation the shell is axially loaded with a uniform prescribed velocity. The assumption of constant velocity is based on high-speed camera observations on the deformation of several shells [1,7,8]. It is presumed that strain rates associated with the unperturbed motion are dominant so that no strain-rate reversal occurs until buckling has well developed. The von Mises yield criterion and the isotropic strain hardening are envisaged. Finally, elastic strains are neglected and deformations are regarded as isochoric. A solution of the governing equations is given for the case of constant nominal strain rate or velocity to provide simple formulas for the preferred buckling mode. In [7,8] the preferred buckling mode is determined numerically by the amplification of initial imperfection for linear hardening materials. Here a closed-form expression for the growth rate of a perturbation of a given wavelength is derived for a thermoviscoplastic cylindrical shell.

We apply the axial velocity V to the ends of a shell to create a uniform stress field σ_x, σ_θ and strain rate field $\dot{\varepsilon}_x, \dot{\varepsilon}_\theta$. Subscripts x and θ denote, respectively, the axial and the circumferential directions. Let the inward radial displacement be $w(x,t)$. Assuming that the sides of the shell elements formed by planes perpendicular to the shell axis remain plane during longitudinal bending, the strain rate in the thin shell is given by Florence and Goodier [7] and Lindberg and Florence [8]

$$\dot{\varepsilon}_x = \dot{\varepsilon}_{x0} + z\frac{\partial^3 w}{\partial t \partial x^2}, \quad \dot{\varepsilon}_\theta = \left(1 - \frac{z}{R}\right)\left(\dot{\varepsilon}_{\theta 0} - \frac{1}{R}\frac{\partial w}{\partial t}\right), \tag{1}$$

where $\dot{\varepsilon}_{x0} = -\dot{\varepsilon}_0 = -V/L$, $\dot{\varepsilon}_{\theta 0} = -\dot{\varepsilon}_{x0}/2$, $\dot{\varepsilon}_{x0}$, $\dot{\varepsilon}_{\theta 0}$ and $\dot{\varepsilon}_0$ are the axial, the circumferential and the effective strain rate on the middle surface of the shell, respectively, z is the radial distance from the midsurface, and R and L are the radius and the length of the shell, respectively.

It has been tacitly assumed in Eq. (1) that $\sigma_{\theta 0} = 0$. Recent three-dimensional (3D) analysis [19–22] of the stress state of the shell has revealed that it is in a biaxial stress state, i.e.,$\sigma_x \neq 0$, $\sigma_\theta \neq 0$, $\sigma_z = 0$, during the early stages of deformation. However, it was shown in [19] that stress states with $\sigma_\theta = 0$ do exist for particular combinations of shell geometries, material properties and loading types and it was explained using stress wave propagation. Generally, the assumption $\sigma_{\theta 0} = 0$ is appropriate as small radial displacements and a sustained plastic flow are prevalent during the impact event.

The incompressibility condition is

$$\dot{\varepsilon}_x + \dot{\varepsilon}_\theta + \dot{\varepsilon}_z = 0. \tag{2}$$

Following [7,8], the effective strain rate is given by

$$\dot{\varepsilon}^2 = \tfrac{2}{3}(\dot{\varepsilon}_x^2 + \dot{\varepsilon}_\theta^2 + \dot{\varepsilon}_z^2) \tag{3}$$

and stress components derived from the flow rule associated with the von Mises yield criterion can be written as

$$\sigma_x = \frac{2(2\dot{\varepsilon}_x + \dot{\varepsilon}_\theta)\sigma}{3\dot{\varepsilon}}, \quad \sigma_\theta = \frac{2(2\dot{\varepsilon}_\theta + \dot{\varepsilon}_x)\sigma}{3\dot{\varepsilon}}, \tag{4}$$

where σ is the effective stress.

In the following formulae, terms with powers of z/R higher than one and terms involving products of displacements have been neglected. Thus, by substituting from Eqs. (1) and (2) into Eq. (3), the effective strain rate is given by

$$\dot{\varepsilon}^2 = \dot{\varepsilon}_0^2 + 2\dot{\varepsilon}_0\left(\frac{2}{3R}\frac{\partial w}{\partial t} - R\frac{\partial^3 w}{\partial t \partial x^2}\right)\frac{z}{R} \tag{5}$$

or equivalently

$$\dot{\varepsilon} = \dot{\varepsilon}_0 + \left(\frac{2}{3R}\frac{\partial w}{\partial t} - R\frac{\partial^3 w}{\partial t \partial x^2}\right)\frac{z}{R}, \tag{6}$$

which can be integrated to give

$$\varepsilon = \varepsilon_0 + \left(\frac{2w}{3R} - R\frac{\partial^2 w}{\partial x^2}\right)\frac{z}{R}. \tag{7}$$

Eq. (7) differs from the corresponding equation in [7,8] because the effect of initial imperfection is included in [7,8].

A constitutive relation is needed for further analysis. Whereas a linear relation between the stress and the strain is assumed in [7,8], a general relation is considered in [13]. For a thermo-viscoplastic material, $\sigma = \sigma(\varepsilon, \dot{\varepsilon}, \theta)$ where θ is the temperature. For high-speed impact under the assumptions of constant strain rate, fixed portion of plastic work converted into heating, and negligible heat loss, it can be reduced [13] to $\sigma = \sigma(\varepsilon)$. Hence for infinitesimal strain increment ε,

$$\sigma = \sigma_0 + E(\varepsilon)\varepsilon, \tag{8}$$

where $E(\varepsilon) = \mathrm{d}\sigma(\varepsilon)/\mathrm{d}\varepsilon$ is the equivalent hardening modulus and σ_0 the stress level intersected on the stress axis by the tangent to the stress–strain curve, as shown in Fig. 1.

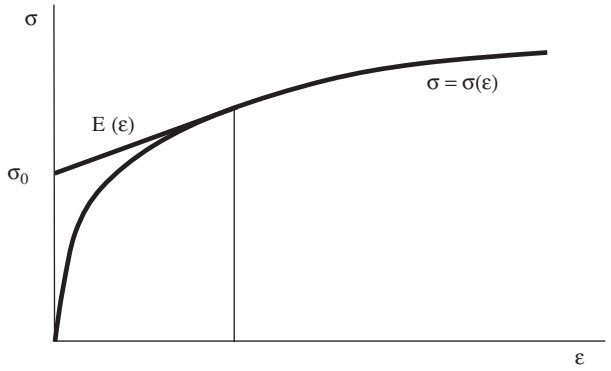

Fig. 1. Schematic stress–strain curve.

Substitution from Eq. (7) into Eq. (8) gives

$$\sigma = \sigma^0 + E(\varepsilon)\left(\frac{2w}{3R} - R\frac{\partial^2 w}{\partial x^2}\right)\frac{z}{R}, \tag{9}$$

where σ^0 is the stress at the midsurface of the shell. From Eqs. (1), (6), (9) and (4), we obtain the following expressions for the stress components:

$$\begin{aligned}\sigma_x = & -\left(1 + \frac{2}{3R\dot{\varepsilon}_0}\frac{\partial w}{\partial t}\right)\sigma^0 - \left[\frac{\sigma^0}{3}\left(1 - \frac{4}{R\dot{\varepsilon}_0}\frac{\partial w}{\partial t} - \frac{R}{\dot{\varepsilon}_0}\frac{\partial^3 w}{\partial t \partial x^2}\right)\right. \\ & \left. + E(\varepsilon)\left(\frac{2w}{3R} - R\frac{\partial^2 w}{\partial x^2}\right)\right]\frac{z}{R}, \\ \sigma_\theta = & -\frac{4\sigma^0}{3\dot{\varepsilon}_0}\frac{\partial w}{\partial t} - \frac{2\sigma^0}{3}\left(1 - \frac{2}{R\dot{\varepsilon}_0}\frac{\partial w}{\partial t} - \frac{R}{\dot{\varepsilon}_0}\frac{\partial^3 w}{\partial t \partial x^2}\right)\frac{z}{R}.\end{aligned} \tag{10}$$

The superscript 0 on σ will be omitted in the following expressions for the ease in writing.

Adopting the sign convention used in [7,8], stresses have the following resultant forces and moments:

$$\begin{aligned}N_x &= \int_{-h/2}^{h/2} \sigma_x \, \mathrm{d}z = -\left(1 + \frac{2}{3R\dot{\varepsilon}_0}\frac{\partial w}{\partial t}\right)\sigma h, \\ N_\theta &= \int_{-h/2}^{h/2} \sigma_\theta \, \mathrm{d}z = -\frac{4}{3\dot{\varepsilon}_0}\frac{\partial w}{\partial t}\sigma h,\end{aligned} \tag{11}$$

$$\begin{aligned}M_x = & -\int_{-h/2}^{h/2} \sigma_x z \, \mathrm{d}z = \frac{h^3}{36R}\left[\sigma\left(1 - \frac{4}{R\dot{\varepsilon}_0}\frac{\partial w}{\partial t} - \frac{R}{\dot{\varepsilon}_0}\frac{\partial^3 w}{\partial t \partial x^2}\right)\right. \\ & \left. + E(\varepsilon)\left(\frac{2w}{R} - 3R\frac{\partial^2 w}{\partial x^2}\right)\right],\end{aligned}$$

$$M_\theta = -\int_{-h/2}^{h/2} \sigma_\theta z \, dz = \frac{h^3\sigma}{18R}\left(1 - \frac{2}{R\dot{\varepsilon}_0}\frac{\partial w}{\partial t} - \frac{R}{\dot{\varepsilon}_0}\frac{\partial^3 w}{\partial t \partial x^2}\right). \tag{12}$$

Here h is the thickness of the shell.

The equation of the transverse motion of a thin cylindrical shell deformed axisymmetrically is [7,8]

$$\frac{\partial^2 M_x}{\partial x^2} + N_x\frac{\partial^2 w}{\partial x^2} + \frac{N_\theta}{R} = \rho h\frac{\partial^2 w}{\partial t^2}, \tag{13}$$

where ρ is the mass density. After substituting from Eqs. (11) and (12) for forces and moments into Eq. (13), we arrive at

$$\frac{\partial^2 w}{\partial t^2} + a\frac{\partial w}{\partial t} + b\frac{\partial^2 w}{\partial x^2} + c\frac{\partial^3 w}{\partial t \partial x^2} + d\frac{\partial^5 w}{\partial t \partial x^4} + e\frac{\partial^4 w}{\partial x^4} = 0, \tag{14}$$

where

$$a = \frac{4\sigma}{3\rho R^2\dot{\varepsilon}_0}, b = \frac{1}{\rho}\left(\sigma - \frac{E(\varepsilon)h^2}{18R^2}\right), c = \frac{\sigma h^2}{9\rho R^2\dot{\varepsilon}_0}, d = \frac{\sigma h^2}{36\rho\dot{\varepsilon}_0}, e = \frac{E(\varepsilon)h^2}{12\rho}.$$

By letting the radius R approach infinity in Eq. (14), we obtain the corresponding equation for a flat plate. The buckling modes of a thin anisotropic plate under impact loading have been studied by Batra and Wei [13]. Furthermore, by omitting the directional longitudinal bending term in Eq. (14), we obtain the following equation for a rod [9]:

$$\frac{\partial^2 w}{\partial t^2} + \tilde{b}\frac{\partial^2 w}{\partial x^2} + \tilde{e}\frac{\partial^4 w}{\partial x^4} = 0, \tag{15}$$

where $\tilde{b} = \sigma/\rho, \tilde{e} = E(\varepsilon)h^2/12\rho$, and h is related to the radius of the rod.

2.2. Buckling modes

In order to find the buckling mode we perturb the deformed state of the cylindrical shell by an infinitesimal amount as has been done in Refs. [1,7]. If the superimposed perturbations grow with time, then the deformed state is assumed to have buckled, and the buckled shape of the shell corresponds to the wavelength of the perturbation that results in the maximum initial growth rate of the perturbation.

Let $w_0(x) = w(x, t_0)$ give the deflection of the shell at time $t = t_0$, $\varepsilon_0 = \dot{\varepsilon}_0 t_0$ the axial strain at time t_0, and an infinitesimal perturbation $\delta w(x, t)$ where $\sup_{0\leqslant x\leqslant L}|\delta w/w_0| \ll 1$ and $\sup_{0\leqslant x\leqslant L}|\delta\dot{w}/\dot{w}_0| \ll 1$, be added to it. We assume that the resultant forces and moments are unaffected by the superimposed perturbation. Also, the perturbation field satisfies the following boundary conditions at the edges of the shell:

$$\delta w(0, t) = \delta w(L, t) = 0, \tag{16}$$

$$\left.\frac{\partial^2 \delta w(0, t)}{\partial x^2}\right|_{(0,t)} = \left.\frac{\partial^2 \delta w(a, t)}{\partial x^2}\right|_{(L,t)} = 0. \tag{17}$$

The perturbation field

$$\delta w(x,t) = \delta w^* e^{\eta(t-t_0)} \sin(\omega x), \quad \omega = 2\pi n/L, \tag{18}$$

where n is an integer, satisfies boundary conditions (16) and (17). There are numerous other perturbations that satisfy boundary conditions (16) and (17). However, they are not considered here. In Eq. (18), η is the initial growth rate of the perturbation at time $t = t_0$ and ω is the wavenumber. A positive value of η implies that the deformed shell at time t_0 is unstable; otherwise it is stable. Substituting $w = w_0 + \delta w$ into Eq. (14) and subtracting Eq. (14) from the resulting equation, we get the following algebraic equation relating the wave number ω to the initial growth rate η:

$$\eta^2 + (a - c\omega^2 + d\omega^4)\eta + (-b\omega^2 + e\omega^4) = 0. \tag{19}$$

In order to find the wavelength for which the growth rate of perturbation is maximum we set

$$\frac{\partial \eta}{\partial \omega^2} = 0. \tag{20}$$

Differentiating both sides of Eq. (19) with respect to ω^2 and using Eq. (20) we obtain

$$\omega^2 = \frac{c\eta + b}{2(d\eta + e)} \quad \text{or} \quad \eta = \frac{2e\omega^2 - b}{c - 2d\omega^2}, \tag{21}$$

where we have tacitly assumed that the denominators do not vanish; a similar assumption is made in the equations to follow. Substituting from Eq. (21) into Eq. (19), we obtain the following two cubic algebraic equations for the initial growth rate and the wavelength:

$$\begin{aligned} &\eta^3 + f_1\eta^2 + f_2\eta + f_3 = 0, \\ &\omega^6 + g_1\omega^4 + g_2\omega^2 + g_3 = 0, \end{aligned} \tag{22}$$

where

$$f_1 = \frac{4(e + ad) - c^2}{4d}, f_2 = \frac{4ae - 2bc}{4d}, f_3 = \frac{-b^2}{4d},$$

$$g_1 = \frac{4e(e - ad) - c(ce - bd)}{2d(ce - bd)}, g_2 = \frac{2a(ce + bd) - 4be}{2d(ce - bd)}, g_3 = \frac{b^2 - abc}{2d(ce - bd)}.$$

Note that b and e are evaluated at $\varepsilon = \varepsilon_0$. The cubic Eq. (22) has either one real root and two complex conjugate roots, or three real roots of which at least two are equal, or three different real roots according as $(p_1/3)^3 + (q_1/2)^3$ and $(p_2/3)^3 + (q_2/2)^3$ are positive, zero, or negative, respectively. Here $p_1 = -f_1^2/3 + f_2$, $q_1 = 2(f_1/3)^3 - (f_1 f_2)/3 + f_3$, $p_2 = -g_1^2/3 + g_2$, $q_2 = 2(g_1/3)^3 - (g_1 g_2)/3 + g_3$. If $(p_1/3)^3 + (q_1/2)^3 \geqslant 0$, and $(p_2/3)^3 + (q_2/2)^3 \geqslant 0$ then the only one real root of the cubic Eqs. (22) is given by

$$\begin{aligned} \eta &= \sqrt[3]{-q_1/2 + \sqrt{(p_1/3)^3 + (q_1/2)^2}} + \sqrt[3]{-q_1/2 - \sqrt{(p_1/3)^3 + (q_1/2)^2}} - f_1/3, \\ \omega^2 &= \sqrt[3]{-q_2/2 + \sqrt{(p_2/3)^3 + (q_2/2)^2}} + \sqrt[3]{-q_2/2 - \sqrt{(p_2/3)^3 + (q_2/2)^2}} - g_1/3. \end{aligned} \tag{23}$$

If $(p_1/3)^3+(q_1/2)^3<0$ and $(p_2/3)^3+(q_2/2)^3<0$ then the three real roots of the cubic Eqs. (22) are given by

$$\begin{aligned}
&\eta_1 = 2\sqrt{(-p_1/3)}\cos(\alpha_1/3),\\
&\eta_2,\eta_3 = -2\sqrt{(-p_1/3)}\cos(\alpha_1/3\pm 60^\circ),\\
&\omega_1^2 = 2\sqrt{(-p_2/3)}\cos(\alpha_2/3),\\
&\omega_2^2,\omega_3^2 = -2\sqrt{(-p_2/3)}\cos(\alpha_2/3\pm 60^\circ),
\end{aligned} \tag{24}$$

where

$$\cos\alpha_1 = -q_1\Big/2\sqrt{-(p_1/3)^3},\quad \cos\alpha_2 = -q_2\Big/2\sqrt{-(p_2/3)^3}.$$

We note that which one of the three values of ω corresponds to η_1 is determined from Eq. (21). For a rod with deformations governed by Eq. (15), the analog of Eqs. (23) and (24) is

$$\eta = \frac{\sqrt{3}\sigma}{h\sqrt{\rho E}},\quad \omega = \frac{\sqrt{6}}{h}\sqrt{\frac{\sigma}{E}}. \tag{25}$$

From Eq. (25) we conclude that the initial growth rate of the perturbation and the corresponding wavenumber increase with an increase in the value of the initial axial stress and a decrease in the hardening modulus. Moreover, the initial growth rate increases with a decrease of the mass density but the wavenumber is independent of mass density.

Should ω computed from Eq. (24) be such that $\omega L/2\pi$ is not an integer then an integer just below $\omega L/2\pi$ or just above it that gives the higher value of η is chosen.

Recalling expressions for a, b, c, d and e given after Eq. (14) and those for f_1, f_2, f_3, g_1, g_2 and g_3 given before Eq. (23), we see that the maximum initial growth rate η and the corresponding wavenumber ω of perturbations depend upon the length of the cylindrical shell and the prescribed axial velocity V only through $\dot{\varepsilon}_0 = V/L$. Thus for a prescribed nominal axial strain rate $\dot{\varepsilon}_0$, the buckling of a cylindrical shell is not affected by the aspect ratio L/R.

2.3. Comparison of predicted buckling mode with experimental observations

Florence and Goodier [7] have experimentally studied the dynamic plastic buckling of cylindrical shells made of 6061-T6 aluminum alloy. Material parameters for their tests are:

$$\rho = 2700\,\mathrm{kg/m^3},\quad \sigma_0 = 307\,\mathrm{MPa},\quad E = 724\,\mathrm{MPa}. \tag{26}$$

Geometric parameters and test results are given in Table 1. For each one of the 24 configurations tested by Florence and Goodier [7], the half wavenumber computed from the present analysis, with the perturbation introduced at time $t_0 = 0.1/\dot{\varepsilon}_0$, is also listed in Table 1. For the first 20 test configurations, it differs from the experimentally observed one by less than 33%. Possible reasons for this discrepancy are: (i) the assumption of homogeneous axisymmetric deformations, (ii) neglect of initial imperfections, (iii) ignoring in expressions (1) and (5) for strains terms of order higher than one in z/R, and (iv) the simple form (18) of the presumed perturbation. A real structure most likely has numerous randomly distributed perturbations of different magnitudes.

Table 1
Observed and predicted number of half waves for cylindrical shells

Shell number	Radius R (cm)	Thickness h (cm)	Length L (cm)	Velocity (m/s)	Average axial strain rate (1/s)	Number of half-waves		
						Experiment	Predicted in [2]	Present analysis
1,2,3,4	1.147	0.241	7.62	101	1325.5	8	10	12
5	1.143	0.254	10.16	53	521.7	12	13	16
6	1.143	0.254	10.16	58	570.9	12	13	15
7	1.143	0.254	10.16	63	620.1	12	13	15
8	1.147	0.241	10.16	78	767.7	12	13	16
9	1.143	0.254	10.16	87	856.3	12	13	15
10	1.143	0.254	10.16	88	866.1	12	13	15
11	1.143	0.254	10.16	99	974.4	12	13	15
12	1.143	0.254	10.16	100	984.3	12	13	15
13,14,15	1.147	0.241	10.16	104	1023.6	12	14	16
16	1.143	0.254	10.16	115	1131.9	11	13	15
17	1.143	0.254	10.16	120	1181.1	11	13	15
18	1.143	0.254	10.16	121	1190.9	12	13	15
19	1.143	0.254	10.16	122	1200.8	11	13	15
20	1.143	0.254	10.16	125	1230.3	12	13	14
21	1.147	0.241	15.24	40	262.5	—	21	24
22	1.147	0.241	15.24	75	492.1	14	21	24
23,24	1.147	0.241	15.24	94	616.8	15	21	24

2.4. Influence of parameters on buckling mode

In order to calculate the hardening modulus $E(\varepsilon)$ for a thermoviscoplastic material we assume that it obeys the following Litonski–Batra thermoviscoplastic relation [23]:

$$\sigma = \sigma_*\left(1+\frac{\varepsilon}{\varepsilon_y}\right)^{\tilde{n}}(1+B\dot{\varepsilon})^m\left(\frac{\tilde{\theta}_m-\tilde{\theta}}{\tilde{\theta}_m-\tilde{\theta}_r}\right)^v, \tag{27}$$

where σ is the effective stress, ε the effective plastic strain, $\dot{\varepsilon}$ the effective plastic strain rate, $\tilde{\theta}$ the temperature, and σ_*, ε_y, B, $\tilde{\theta}_m$, $\tilde{\theta}_r$, m, $\tilde{n}$ and v are material parameters.

During a relatively high strain rate loading process deformations can be assumed to be locally adiabatic. A part of the plastic work is converted into heat causing the temperature to rise. For locally adiabatic deformations, the evolution of temperature is given by

$$\frac{\mathrm{d}\tilde{\theta}}{\mathrm{d}\varepsilon} = \frac{\beta\sigma}{\rho C}, \tag{28}$$

where $0<\beta<1$ and C is the specific heat. For most metals, $0.85<\beta<0.95$.

Suppose that the strain rate is constant. Substitution for σ from Eq. (27) into Eq. (28) and integration of the resulting equation give

$$\tilde{\theta} = \tilde{\theta}_m-(\tilde{\theta}_m-\tilde{\theta})\exp\left\{-\frac{\beta\sigma_*\varepsilon_y(1+B\dot{\varepsilon})^m}{\rho C(\theta_m-\theta_r)(\tilde{n}+1)}\left[\left(1+\frac{\varepsilon}{\varepsilon_y}\right)^{\tilde{n}+1}-1\right]\right\} \quad \text{for} \quad v=1, \tag{29}$$

$$\tilde{\theta} = \tilde{\theta}_m-\left\{(\tilde{\theta}_m-\tilde{\theta}_r)^{1-v}-\frac{\beta(1-v)\sigma_*\varepsilon_y(1+B\dot{\varepsilon})^m}{\rho C(\theta_m-\theta_r)^v(\tilde{n}+1)}\left[\left(1+\frac{\varepsilon}{\varepsilon_y}\right)^{\tilde{n}+1}-1\right]\right\}^{1/1-v} \quad \text{for} \quad v\neq 1. \tag{30}$$

Thus the hardening modulus, shown in Fig. 1, is given by

$$E(\varepsilon) = \frac{\mathrm{d}\sigma}{\mathrm{d}\varepsilon} = \frac{\partial\sigma}{\partial\varepsilon}+\frac{\partial\sigma}{\partial\tilde{\theta}}\frac{\mathrm{d}\tilde{\theta}}{\mathrm{d}\varepsilon}. \tag{31}$$

The terms in Eq. (31) can be evaluated by using Eq. (27) and either Eq. (29) or Eq. (30).

Henceforth we assume that the body is made of HY-100 steel. Values of material and geometric parameters are listed in Table 2.

Table 2
Values of material and geometric parameters

β	$\dot{\varepsilon}_0$ (1/s)	ρ (kg/m^3)	$\tilde{n}$	m	$\tilde{\theta}_m$ (K)	$\tilde{\theta}_r$ (K)
0.9	1000	7860	0.107	0.0117	1500	300
C (J/kg K)	B (s^{-1})	ε_y	σ_* (MPa)	R (mm)	h (mm)	v
473	17320	0.007	405	11.43	2.54	1.0

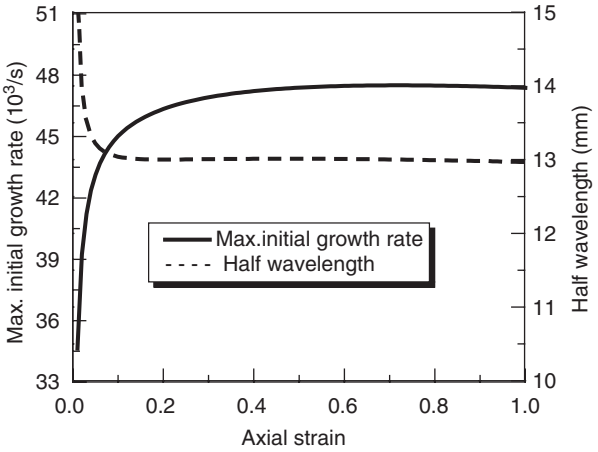

Fig. 2. Dependence of the maximum initial growth rate of perturbation and the corresponding half-wavelength upon the nominal strain when the homogeneously deformed shell is perturbed.

Fig. 2 shows the dependence of the maximum initial growth rate of perturbation and the corresponding half-wavelength, defined as π/ω, upon the nominal axial strain when the deformed shell is perturbed. It is found that with an increase in the initial strain, the growth rate increases dramatically at first and soon reaches a plateau. The corresponding half-wavelength exhibits a similar behavior except that it decreases slowly. Although buckling initiates at a small strain with a small half-wavelength, however, in dynamic deformations the initial buckling mode may not prevail since the strain increases rapidly with time and the preferential wavelength may change during the deformation process. Hence the final buckled shape will depend on the entire loading history. However, it was observed in [7,8] that the buckling mode was selected very early in the deformation process. Without knowing full details of the experiment, henceforth we choose the buckling mode that corresponds to the perturbation introduced at an initial axial strain of 0.1, and delineate the influence of different parameters on the buckling mode. The hardening modulus given by Eq. (31) is evaluated at $\varepsilon = 0.1$. While conducting the parametric study, only one variable is varied at a time, others are assigned values listed in Table 2, and the nominal axial strain rate equals 1000/s.

Fig. 3a–g exhibits the influence of the strain hardening exponent, strain rate hardening exponent, shell wall thickness, thermal softening exponent, strain rate, mass density and the hardening modulus on the half-wavelength of the buckled shape. Results are obtained by using Eq. (24). The half-wavelength increases monotonically with an increase in the radius of the shell, the shell wall thickness, the strain hardening exponent and the strain rate hardening exponent, and decreases monotonically with an increase in the applied strain rate, the mass density and the thermal softening exponent. A large value of the half-wavelength implies that the cylindrical shell will buckle as a column. Fig. 3d also evinces that the larger inertia associated with the higher value of the mass density makes the half-wavelength smaller. We note that Florence and Goodier [7] tested only aluminum alloy cylindrical shells, and the range of strain rates considered is too small to compare their results with those of Fig. 3c. Moreover, aluminum is usually less strain-rate sensitive than steel.

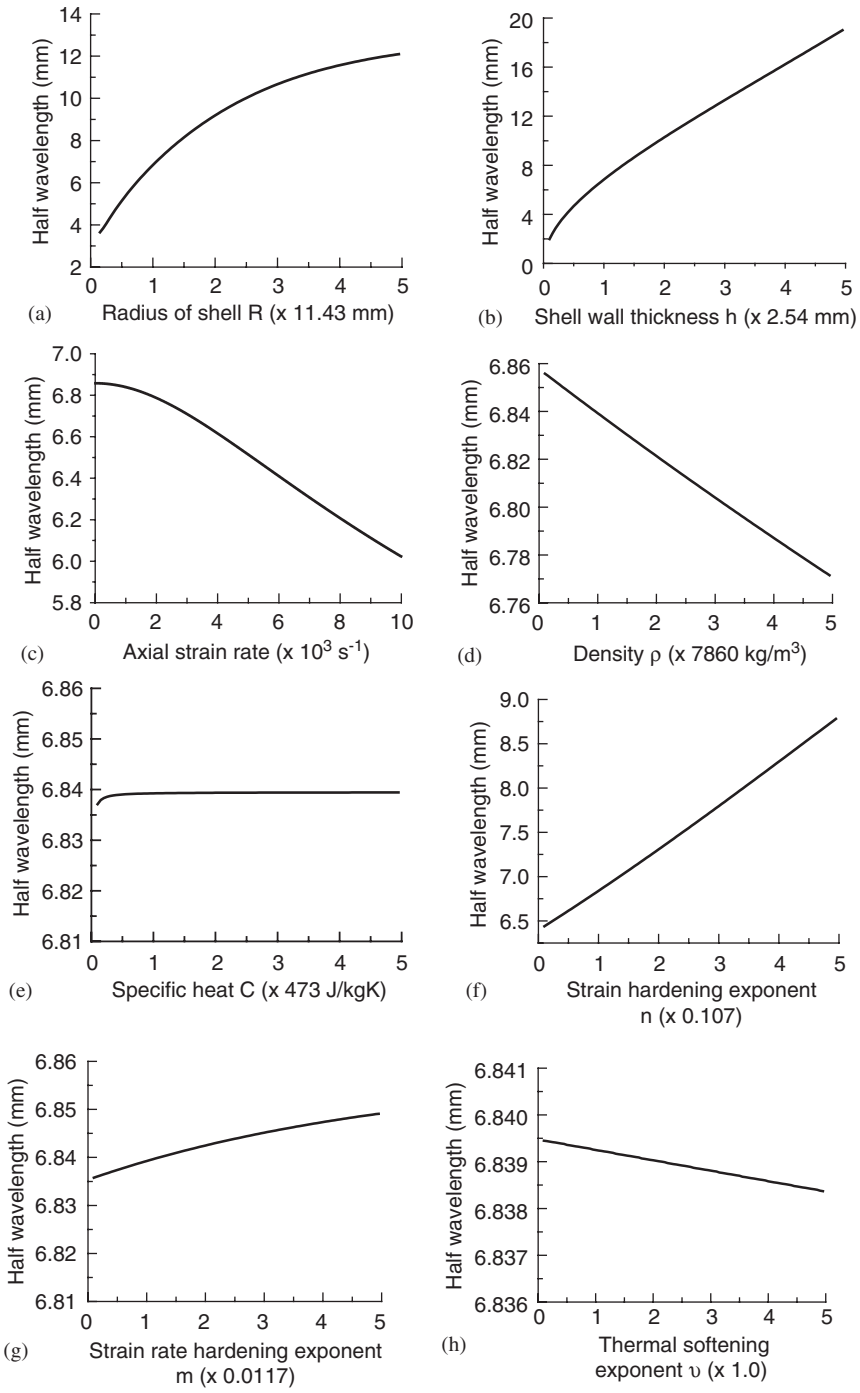

Fig. 3. Dependence of the half wavelength of the buckled shell upon (a) radius of the shell, (b) shell wall thickness, (c) nominal strain-rate, (d) mass density, (e) specific heat, (f) strain-hardening exponent, (g) strain-rate hardening exponent, and (h) thermal softening exponent.

3. Dynamic plastic buckling analyzed by the finite element method

Dynamic plastic buckling can develop at high strain rates while dynamic progressive buckling dominates the shell response for a wide range of loading and material parameters especially at low to moderate strain rates [1]. Dynamic plastic buckling is characterized by an initial wrinkling within a sustained plastic flow along the shell length during the initial phase of deformation, but the strain localizes in the case of progressive buckling. In this section, the buckling behavior of cylindrical shells under relatively low speed of impact is studied by the finite element method (FEM).

The shell is made of an aluminum alloy that is taken to be homogeneous, isotropic, incompressible and elastic–plastic with a mass density of 2700 kg/m^3. Its Young's modulus, yield stress and hardening modulus are 72 GPa, 320 MPa and 426 MPa, respectively. The strain rate effect is not considered because the aluminum alloy is strain-rate insensitive. Note that in the perturbation analysis of Section 2, elastic deformations and strain-rate reversals were neglected. The geometric and material properties used in the simulation are assigned the following values: the length is 60 mm, the radius of the middle surface is 10 mm, the thickness is 1.0 mm. In simulations, the shells are sandwiched between two rigid platens. The top platen moves downward with an axial velocity of 10 m/s, while the bottom platen is stationary. Thus deformations are not symmetric about the horizontal plane passing through the centroid of the shell, and the nominal strain rate equals 167/s. All contacts, including contact between the shell and the platens, and the contact between folded surfaces of the shell when they have developed are assumed to be frictionless. No constraints are applied to nodes at the distal and the proximal ends and the shell is regarded as simply supported. The numerical simulation is carried out using the FE code MSC/Dytran. Several test simulations were performed to determine the proper mesh density and the element size. These exercises suggested that the entire shell be divided into 2500 Belytschko–Lin–Tsay shell elements and nine integration points be used to evaluate domain integrals. The effects

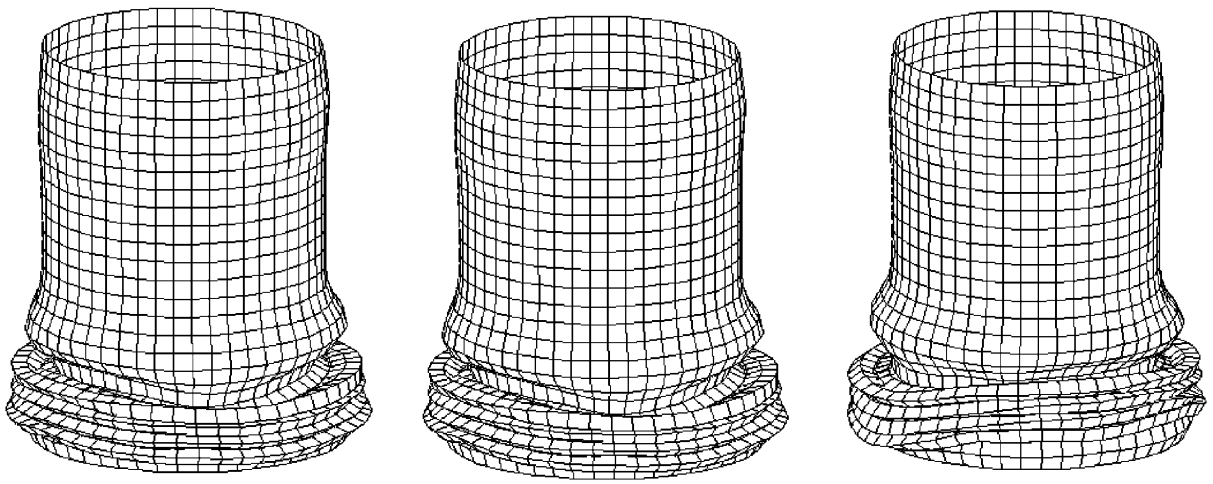

Fig. 4. Buckled cylindrical shells with 3 different random distributions of imperfections (5 seeds).

of imperfections have been simulated by many investigators, e.g. see [18]. However, these were not considered in [19–22] wherein the effects of the stress wave propagation on the buckling behavior were studied in detail. In all numerical simulations reported in [19–22], the axisymmetric buckling mode was assumed and 2D axisymmetric solid elements were used. Here, due to the presence of imperfections and different boundary conditions at the end faces, the deformation is asymmetric, so the entire shell is simulated. The influence of imperfections is investigated.

In the automotive industry mechanically imposed triggers are often used to control the behavior of the energy absorber during axial loading. When an imperfection is introduced, asymmetric deformations appear. Fig. 4 shows three typical buckled shapes of the aluminum alloy shells at a

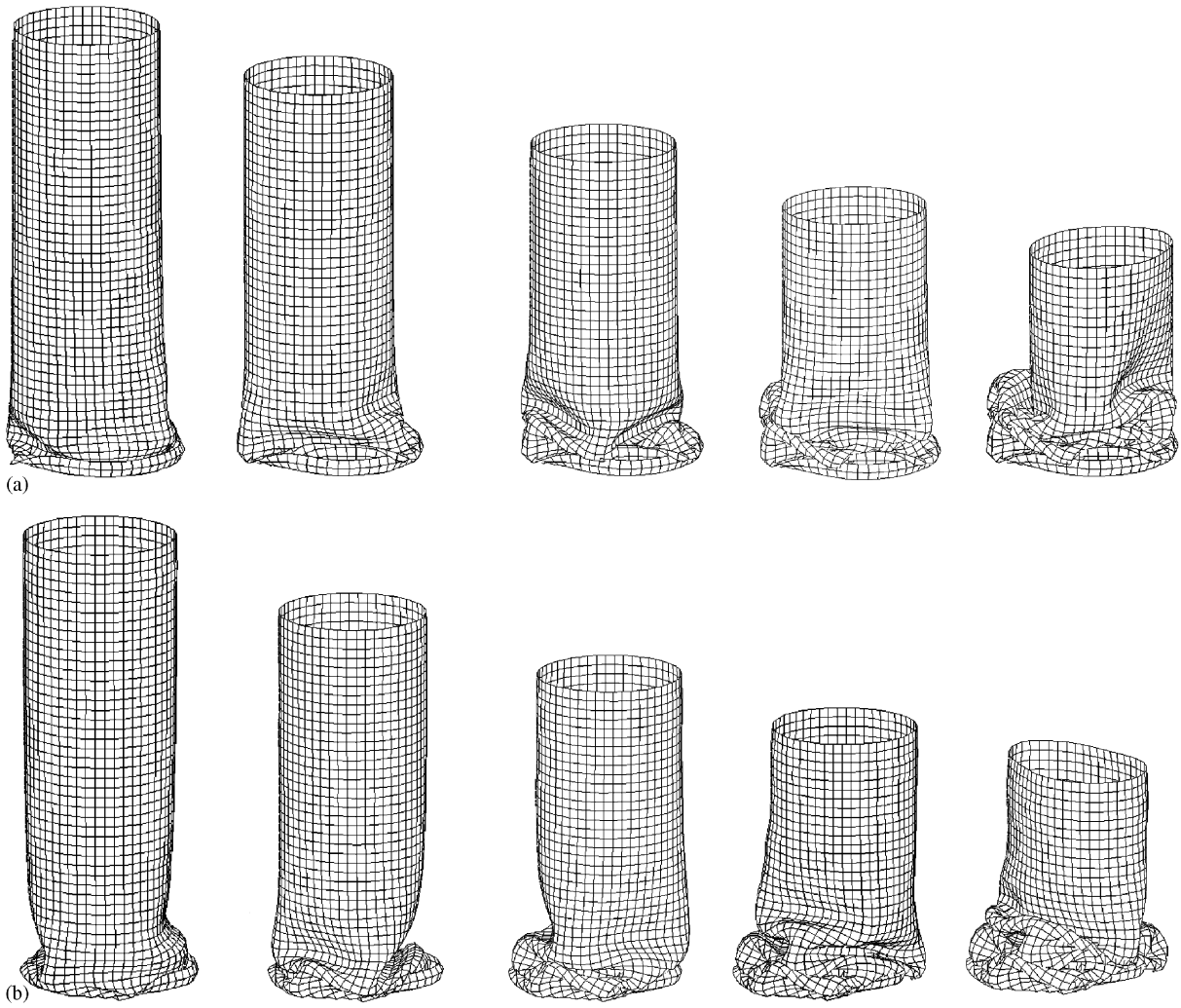

Fig. 5. Buckled shapes of cylindrical shells with 2 different randomly distributed imperfections (50 seeds) at $\Delta L/L_0 = 0.116$, 0.232, 0.348, 0.464, 0.58, respectively.

deformation of $\Delta L/L_0 = 0.6$, where ΔL and L_0 are the axial displacement of the top end and the initial length of the shell, respectively. These simulations are with different random imperfections in the form of 30% reduction in the thickness of shell elements. This initial perturbation is quite different from that considered in Section 2. Different random distributions alter the deformed configurations but do not significantly change the development of the buckling mode. Fig. 5 shows other 2 typical examples of the buckled shapes for aluminum alloy shells at different levels of deformation obtained with 50 different random imperfections. It is evident that more imperfections result in a stronger asymmetric deformation than that observed in Fig. 4. All shells buckle progressively, with buckling initiating from the distal end.

A quantity of particular interest in the buckling analysis is the axial force as a function of the axial displacement. The axial forces at the two end faces of a shell are computed and it is found that there is no noticeable difference between the forces endured at distal and proximal ends due

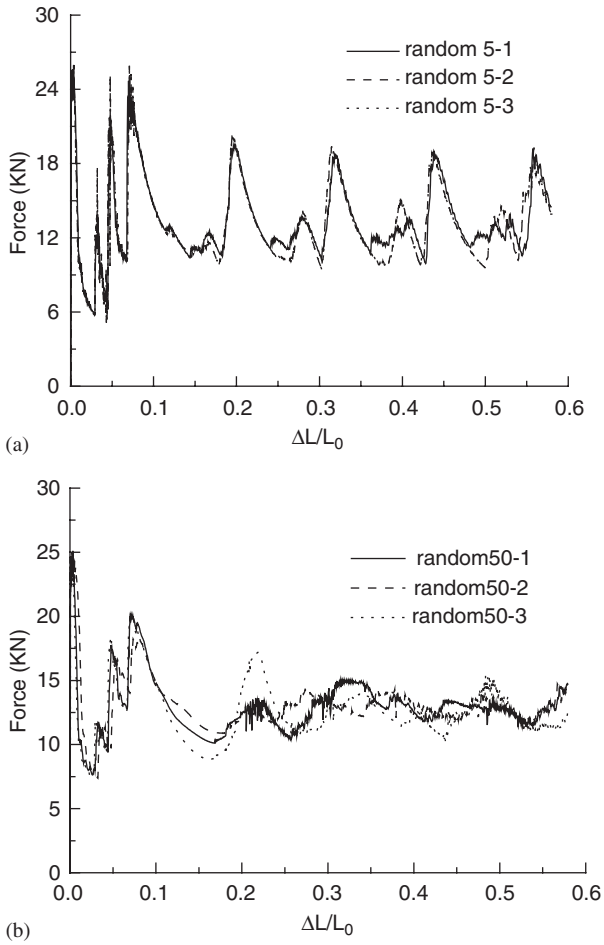

Fig. 6. Force-deformation histories for cylindrical shells with 3 different random distributions of imperfections; (a) 5 seeds, and (b) 50 seeds.

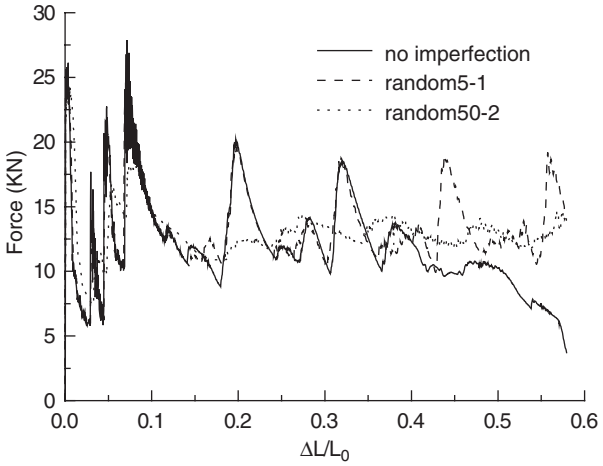

Fig. 7. Comparison of the force-deformation histories for shells with 2 different random distributions of imperfections (5 and 50 seeds) and that without any imperfection.

to the relatively low impact speed. Fig. 6 shows the force–deformation histories for 3 different random distributions of imperfections, results plotted in Fig. 6a are with 5 imperfections and those in Fig. 6b are with 50 imperfections. It is found that the number of imperfections rather than their locations determines the force–deformation curve. The number of peaks in the load–displacement curve is more for 5 defects than those for 50 defects. Also, the magnitude of each peak load is higher for 5 defects than that for 50 defects; however, the average value of the axial load during the deformation process is nearly the same. Thus the energy absorbed by the shell for the same axial strain is virtually unaffected by the number of defects. Fig. 7 shows a comparison of the force–deformation histories for random distributions of 5 and 50 imperfections and that without any imperfection. It is evident that, by introducing a large number of initial imperfections in the shell the peak load during the initial and the subsequent buckling can be significantly reduced. This conclusion is consistent with that obtained in [18].

4. Conclusions

The dynamic buckling behavior of a thermo-viscoplastic thin circular cylindrical shell with axial velocity prescribed at its end faces is investigated analytically in the first part and numerically in the second part of the paper. In the first part, cubic algebraic equations for the maximum initial growth rate of infinitesimal perturbations superimposed upon a homogeneously deformed state and for the corresponding wavelength are obtained. It is hypothesized that the buckled shape corresponds to this wavelength. The influence of many parameters on the growth rate and the wavelength of the buckling mode is delineated.

In the second part of the paper the buckling behavior of a circular cylindrical shell under relatively low impact speed and containing initial imperfections is studied using the finite element method. Two mechanisms of buckling initiation are observed for the shell geometry analyzed: dynamic plastic buckling, when the entire length of the shell wrinkles before the development of

large radial displacements, and dynamic progressive buckling, when the shell folds develop sequentially.

Acknowledgements

ZGW and RCB were partially supported by the ONR grant N00014-98-1-0300 to Virginia Polytechnic Institute and State University with Dr. Y.D.S. Rajapakse as the cognizant program manager, and JLY by the National Natural Science Foundation of China (Project No. 90205003). Opinions expressed in the paper are those of the authors and not of funding agencies.

References

[1] Jones N. Structural impact. Cambridge: Cambridge University Press; 1989 Paperback ed. 1997.
[2] Abramowicz W, Jones N. Dynamic axial crushing of circular tubes. Int J Impact Eng 1984;2:263–81.
[3] Reid SR. Plastic deformation mechanism in axially compressed metal tubes used as impact energy absorbers. Int J Mech Sci 1993;35(12):1035–52.
[4] Mikkelsen LP. A numerical axisymmetric collapse analysis of viscoplastic cylindrical shell under axial compression. Int J Solids Struct 1999;36:643–68.
[5] Gupta NK, Abbas H. Some consideration in axisymmetric folding of metallic round tubes. Int J Impact Eng 2001;25:331–44.
[6] Gupta NK, Sekhon GS, Gupta PK. A study of fold formation in axisymmetric axial collapse of round tubes. Int J Impact Eng 2002;27:87–117.
[7] Florence AL, Goodier JN. Dynamic plastic buckling of cylindrical shells in sustained axial compressive flow. J Appl Mech 1968;35(1):80–6.
[8] Lindberg HE, Florence AL. Dynamic pulse buckling-theory and experiment. Martinus Nijhoff Publishers 1987.
[9] Abrahamson GR, Goodier JN. Dynamic flexural buckling of rods within an axial plastic compression wave. J Appl Mech 1966;33:241–7.
[10] Goodier JN. Dynamic buckling of rectangular plates and sustained plastic compressive flow. In: Engineering plasticity. Cambridge: Cambridge University Press; 1968. p. 183–200 Proceedings of an international conference of plasticity, Cambridge, England, March 1968.
[11] Wang R, Ru CQ. An energy criterion for dynamic plastic buckling of circular cylinders under impulsive loading. In: Reid SR, editor. Metal forming and impact mechanics. Oxford: Pergamon Press; 1985. p. 213–24.
[12] Gu W, Tang W, Liu T. Dynamic pulse buckling of cylindrical shells subjected to external impulsive loading. J. Pressure Vessel Technol 1996;118:33–7.
[13] Batra RC, Wei ZG. Dynamic buckling of a thin thermoviscoplastic rectangular plate. J Thin-Walled Struct 2005;43:273–90.
[14] Murase K, Jones N. The variation of modes in the dynamic axial plastic buckling of circular tubes. In: Gupta NK, editor. Plasticity and impact mechanics. New Delhi: Wiley Eastern Limited; 1993. p. 222–37.
[15] Abramowicz W, Jones N. Transition from initial global bending to progressive buckling of tubes loaded statically and dynamically. Int J Impact Eng 1997;19:415–37.
[16] Tam LL, Callandine CR. Inertia and strain rate effects in a simple plate-structure impact loading. Int J Impact Eng 1991;11(3):349–77.
[17] Harrigan JJ, Reid SR, Peng C. Inertia effects in impact energy absorbing materials and structures. Int J Impact Eng 1999;22(9-10):955–79.
[18] Langseth M, Hopperstad OS, Berstad T. Crashworthiness of aluminum extrusions: validation of numerical simulation, effect of mass ratio and impact velocity. Int J Impact Eng 1999;22:829–54.

[19] Karagiozova D, Jones N. Dynamic elastic–plastic buckling of circular cylindrical shells under axial impact. Int J Solids Struct 2000;37(14):2005–34.
[20] Karagiozova D, Alves M, Jones N. Inertia effects in axisymmetrically deformed cylindrical shells under axial impact. Int J Impact Eng 2000;24:1083–115.
[21] Karagiozova D, Jones N. Influence of stress waves on the dynamic plastic and dynamic progressive buckling of cylindrical shells under axial impact. Int J Solids Struct 2001;38:6723–49.
[22] Karagiozova D, Jones N. On dynamic buckling phenomena in axially loaded elastic–plastic cylindrical shells. Int J Non-Linear Mech 2002;37:1223–38.
[23] Batra RC. Steady state penetration of thermoviscoplastic targets. Comput Mech 1988;3:1–12.